



Research Article

Impact of inclined magnetic field on non-orthogonal stagnation point flow of CNT-water through stretching surface in a porous medium

Issa EL GLILI¹, Mohamed DRIOUICH^{1,*}

¹Laboratory of Research in Physics and Engineering Sciences, Faculty of Polydisciplinary, Sultan Moulay Slimane University, Beni Mellal, 23030, Morocco

ARTICLE INFO

Article history

Received: 29 August 2022

Revised: 15 December 2022

Accepted: 11 January 2023

Keywords:

Oblique Stagnation Point; Nanofluid; Stretching Surface; Non-Linear Thermal Radiation; Inclined Magnetic Field; Porous Medium; Heat Transfer

ABSTRACT

The magnetohydrodynamic (MHD) nanofluid flow at non-orthogonal stagnation point, with suspended carbon nanotubes in water on a stretched sheet in a permeable media with non-linear thermal radiation is studied. This work aims to explore the inclined magnetic field impacts on normal velocity, tangential velocity and temperature for both types of carbon nanotubes (CNTs). The governing flow equations which are continuity equation, momentum equation and energy equation are reformed into ordinary differential form with the proper boundary conditions using appropriate transformations. The computational solution of the nonlinear ODEs is obtained using the Bvp4c method. The graphs are presented to show the influence of certain physical factors which ranged as magnetic parameter ($0.5 \leq M \leq 2.5$), inclination angle of the magnetic field ($\pi/2 \leq \zeta \leq \pi/4$), permeability parameter ($0 \leq \Omega \leq 2$), volume fraction of nanoparticle ($0.03 \leq \Phi \leq 0.07$), stretching ration parameter ($0.3 \leq \gamma_2 \leq 0.7$), Radiation parameter ($0.5 \leq Nr \leq 0.9$), the heating parameter ($0.5 \leq \theta_w \leq 1.5$) and Prandtl number ($5 \leq Pr \leq 10$). The normal and tangential velocity drops with the augmentation of (M), (ζ) and (Ω), while the temperature rise with enhance of (Nr) and (θ_w). This study's findings may be used to manage the heat transmission and fluid velocity rate to achieve the required final product quality in numerous manufacturing processes such as electronic cooling, solar heating, biomedical and nuclear system cooling. Validation against previous research available in the literature in specific situations shows excellent agreement.

Cite this article as: El Glili I, Driouich M. Impact of inclined magnetic field on non-orthogonal stagnation point flow of CNT-water through stretching surface in a porous medium. J Ther Eng 2024;10(1):115–129.

INTRODUCTION

The study of point of stagnation has been attracting numerous researchers throughout the history of fluid dynamics by reason of its practical applications for example,

nuclear reactor cooling during an unexpected power failure and cooling electronic equipment. When a fluid flow interacts with a solid wall, the fluid velocity at such point is relatively zero, which is known as point of stagnation. Less focus

*Corresponding author.

*E-mail address: Driouich.cedoc@gmail.com

This paper was recommended for publication in revised form by Ahmet Selim Dalkılıç



has been given to oblique point of stagnation compared to orthogonal stagnation point flows which have been studied by many authors. Wang [1] investigated numerically the unsteady flow of three-dimensional non-orthogonal point of stagnation using the fifth-order RK Fehlberg algorithm. The oblique Axially symmetric point of stagnation flow of a fluid supposed viscous on a circular cylinder by means of coupled ordinary differential equations has been studied by Weidman et al. [2]. The 2D oblique steady flow at the point of stagnation of a viscous incompressible fluid over a stretching surface has been discussed by Reza et al. [3], By varying the stretching parameter of the surface, they found that the ratio of heat exchange at the stretched surface may be enhanced or decreased. Labropulu et al. [4] numerically investigated the oblique flow at the point of stagnation of a fluid considered to be non-Newtonian on a stretched sheet with heat exchange using a quasi-linearization technique, they conclude that the an upsurge in the fluid elasticity lead to enhance the velocity and reduce the temperature. Sarkar et al. [5] studied the slip impacts on the oblique point of flow stagnation over a rough surface of viscous fluid. Awan et al. [6] investigated the unsteady non-orthogonal point of flow stagnation of second-grade fluid across a stretched sheet taking into account the slip effects.

The magnetohydrodynamics (MHD) is the discipline of the dynamics of magnetic fields in an electrically conductive fluid, has been conducted by many scientists and engineers [7–12]. Singh et al. [13] examined the steady two-dimensional, incompressible and viscous fluid flow at oblique point of stagnation hitting over a stretching sheet in the presence of magnetic field and radiative heat. Borrelli et al. [14] examined the 2-D steady flow of a electrically conducting Newtonian fluid at an oblique stagnation point with effect of a uniform external electromagnetic field. In the presence of a uniformly applied magnetic field, an unsteady oblique point of flow stagnation of a viscous fluid over an oscillating flat plate has been investigated by Javed et al. [15], the equations are solved using Keller-box method and they found that because of the oscillating plate and magnetic field, the velocity profile of the Newtonian fluid raised in the non-orthogonal region of the stagnation point only. Awan et al. [16] studied numerically the magnetohydrodynamic impacts of an incompressible two-dimensional unsteady Jeffrey fluid model at an oblique point of flow stagnation driven by an oscillating stretching sheet. Mohamed et al. [17] numerically examined the magnetohydrodynamic (MHD) point of flow stagnation over a stretching sheet of blood based Casson ferrofluid with Newtonian heating and using the model of Tiwari and Das nanofluid. The Fe_3O_4 cobalt ferrite CoFe_2O_4 ferroparticles and ferrite was used for the study. As a result, they found that the stretching parameter play an important role to reduce the difference in surface temperature between cobalt, ferrite blood based Casson ferrofluid and blood based fluid.

Countless applications have been provided to the field of nanofluids ranging from biomedical to chip cooling [18–20].

They are known to significantly increase heat conductivity [21]. The heat exchange efficiency of carbon nanotubes (CNTs) has been proven to be extremely high, in addition to conventional nanofluids that comprise 1-100 nm nanoparticles for heat transfer enhancement reasons. These tubes with diameter measured in nanometer are made from rolled-up graphene sheets. Due to their high thermal conductivities, carbon nanotubes (CNTs) represent a great opportunity for usage as nanofluid additives. SWCNTs are carbon nanotubes with a single surface, whereas MWCNTs have many surfaces. SWCNTs are known to be more effective than MWCNTs because they tend to lose some of their electronic characteristics, whereas SWCNTs are utilized specifically for electronic applications. Although, the benefit of MWCNTs over SWCNTs since they are more rigid, simple and affordable to create on a wide scale. A considerable amount of studies on the nanofluid with magnetohydrodynamics for instance [22–26]. The inclined hydromagnetic flow of nanofluid under thermal radiation close to the point of stagnation through a stretched sheet, and varying viscosity of the nanofluid has been studied by Khan et al. [27]. Mehmood et al. [28] analyzed the oblique point of flow stagnation of an Ethylene- Glycol and water based nanofluid with heat exchange across a stretched sheet, it was found that, in comparison to Ethylene-based nanofluids, water-based nanofluids exhibit local heat flux. Khan et al. [29] studied the oscillatory non-orthogonal point of flow stagnation of MHD nanofluid over a flat plate considering the slip effect, examining three distinct nanoparticles Titania, Copper and Alumina while utilizing water as the working fluid, they observed that Cu nanoparticles, when compared to other nanoparticles examined, can increase the magnetic susceptibility of nanofluids. Nadeem et al. [30] examined the unsteady MHD oblique point of flow stagnation over an oscillatory stretching/shrinking surface of a nanofluid with suction effect. Rizwana et al. [31] numerically studied the MHD oblique point of flow stagnation through a Riga plat of copper-water nanofluid, they conclude that the Riga parameter and Casson parameter increase the velocity field. Ghasemi et al. [32] studied the effects of solar radiation on two-dimensional flow at point of stagnation of MHD nanofluid on a stretched sheet under thermal radiation, Ohmic heating and viscous dissipation. The governing equation was solved using the differential quadrature method (DQM), it was found that the temperature profiles enhanced by decreasing the Prandtl number and enhancing the solar radiation parameter. Zainal et al. [33] used the Bvp4c approach to solve the two-dimensional unsteady flow of MHD hybrid nanofluid ($\text{Al}_2\text{O}_3\text{-Cu/H}_2\text{O}$) at point of stagnation across an exponentially permeable stretching/shrinking sheet. They concluded that raising the suction parameter and the MHD parameter increases the skin friction coefficient and ratio of heat exchange of the hybrid nanofluid. Nandi et al. [34] explored a computational and statistical study of the MHD flow at the point of stagnation of $\text{Fe}_3\text{O}_4/\text{Cu}/\text{Ag-CH}_3\text{OH}$ nanofluid on a heated permeable stretched sheet. With the impact of viscous dissipation, activation energy, velocity

slip, concentration slip, thermophoresis and chemical reaction. The method of Runge-Kutta-Fehlberg was used for the numerical approach. They concluded that the fluid velocity is always lower for Fe₃O₄-CH₃OH and Cu-CH₃OH nanofluids as compared to Ag-CH₃OH nanofluid.

The analytical or numerical solutions in the above studies are examined using the approximation of Rosseland for the thermal radiation, which is the emission of electromagnetic radiations in all directions by a heated substance, since the flow temperature difference is very small, they described T⁴ as a linear function of T. Ghaffari et al. [35] explored the nonlinear radiation impact of viscoelastic fluid on 2-D non-orthogonal point of flow stagnation in a impermeable media; the results of the study are obtained using Iterative Scheme of Chebyshev Spectral Newton they found that small value of surface heating and radiation parameter can control the width of thermal limit layer. Khan et al. [36] investigated the impact of nonlinear thermal radiation on the MHD point of flow stagnation of two Burgers' nanofluids driven by cylinder stretching the solution have been obtained using HAM. The nonlinear radiative heat effects on a point of flow stagnation of MHD Casson nanofluid with boundary conditions of Thompson and Troian slip have been studied by Akaje et al. [37]. Abbasi et al. [38] consider the axisymmetric rotational point of flow stagnation of hybrid nanofluid with effects of activation energy and nonlinear thermal radiation and considering both type of CNTs nanoparticle and water as base fluid, they found that increasing activation energy and nanoparticle volume fraction reduce the concentration of nanoparticles.

Motivated by the above studies, the effects of inclined magnetic field on oblique point of flow stagnation of carbon nanotubes over a stretching surface through permeable medium with nonlinear thermal radiation is examined. The differential partial equations (PDEs) are changed, by applying suitable transformation to the dimensionless ordinary differential equations (ODEs). The bvp4c approach has been used to solve numerically the resulting equations. In an attempt to observe the effect of diverse physical factors on the normal velocity, tangential velocity and temperature, the results were examined graphically. To our best knowledge, no such works have been published which discuss the present problem.

MATHEMATICAL FORMULATION

The 2-D stationary flow of nanofluid at non-orthogonal point of stagnation over a stretched sheet with thermal radiation considered nonlinear. The flow is subjected to a tilted magnetic field B₀ with constant intensity and makes an angle ζ with the y-axis. The induced magnetic field is ignored since it is assumed to be significantly small compared to the external magnetic field. Two identical and opposed forces are employed along the x-axis with velocity u = ex so that the surface is stretched while maintaining the center fixed. We take T_w the surface temperature and T_∞ denote the ambient temperature, as appear in Figure 1.

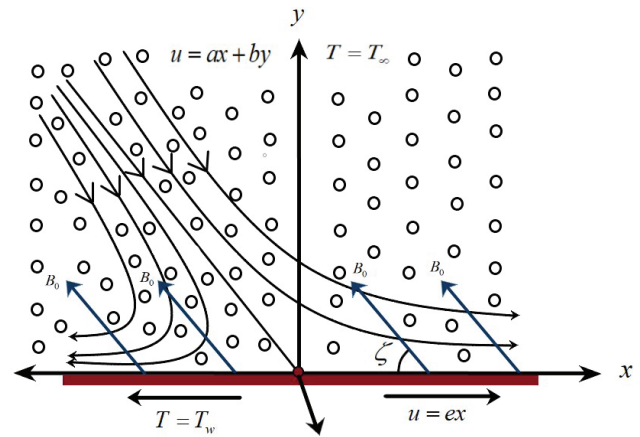


Figure 1. Physical configuration of square duct flow.

Under the above assumptions and considering the fluid in a permeable media, the fluid flow equations can be expressed as [39–41]:

$$\frac{\partial \bar{u}}{\partial \bar{x}} + \frac{\partial \bar{v}}{\partial \bar{y}} = 0 \tag{1}$$

$$\bar{u} \frac{\partial \bar{u}}{\partial \bar{x}} + \bar{v} \frac{\partial \bar{u}}{\partial \bar{y}} = -\frac{1}{\rho_{nf}} \frac{\partial \bar{p}}{\partial \bar{x}} + \nu_{nf} \left(\frac{\partial^2 \bar{u}}{\partial \bar{x}^2} + \frac{\partial^2 \bar{u}}{\partial \bar{y}^2} \right) - \frac{\sigma B_0^2}{\rho_{nf}} \sin^2(\zeta) \bar{u} - \frac{\nu_{nf}}{K} \bar{u} \tag{2}$$

$$\bar{u} \frac{\partial \bar{v}}{\partial \bar{x}} + \bar{v} \frac{\partial \bar{v}}{\partial \bar{y}} = -\frac{1}{\rho_{nf}} \frac{\partial \bar{p}}{\partial \bar{y}} + \nu_{nf} \left(\frac{\partial^2 \bar{v}}{\partial \bar{x}^2} + \frac{\partial^2 \bar{v}}{\partial \bar{y}^2} \right) \tag{3}$$

$$\bar{u} \frac{\partial T}{\partial \bar{x}} + \bar{v} \frac{\partial T}{\partial \bar{y}} = \alpha_{nf} \left(\frac{\partial^2 T}{\partial \bar{x}^2} + \frac{\partial^2 T}{\partial \bar{y}^2} \right) - \frac{1}{(\rho C_p)_{nf}} \frac{\partial q_r}{\partial \bar{y}} \tag{4}$$

where q_r is the thermal radiation and is stated as [40,42,43]:

$$q_r = -\frac{4\sigma^*}{3k^*} \frac{\partial \bar{T}^4}{\partial \bar{y}} = -\frac{16\sigma^*}{3k^*} \bar{T}^3 \frac{\partial \bar{T}}{\partial \bar{y}} \tag{5}$$

The appropriate boundary conditions are,

$$\begin{cases} \bar{u} = e\bar{x} ; \bar{v} = 0 ; \bar{T} = T_w & \text{for } \bar{y} = 0 \\ \bar{u} = a\bar{x} + b\bar{y} ; \bar{T} = T_\infty & \text{for } \bar{y} \rightarrow \infty \end{cases} \tag{6}$$

where \bar{u} and \bar{v} are normal and tangential velocity in x and y-axis respectively.

Simplification of Mathematical Formulation

Introducing these quantities,

$$\begin{aligned} x &= \bar{x} \sqrt{\frac{e}{\nu_f}}; & y &= \bar{y} \sqrt{\frac{e}{\nu_f}}; & p &= \frac{1}{\mu_f e} \bar{p}; \\ u &= \bar{u} \frac{1}{\sqrt{\nu_f e}}; & v &= \bar{v} \frac{1}{\sqrt{\nu_f e}}; & T &= \frac{\bar{T} - T_\infty}{T_w - T_\infty} \end{aligned} \quad (7)$$

Equation (1) to (4) become,

$$\frac{\partial u}{\partial x} + \frac{\partial v}{\partial y} = 0 \quad (8)$$

$$u \frac{\partial u}{\partial x} + v \frac{\partial u}{\partial y} = -\frac{\rho_f}{\rho_{nf}} \frac{\partial p}{\partial x} + \frac{\nu_{nf}}{\nu_f} \left(\frac{\partial^2 u}{\partial x^2} + \frac{\partial^2 u}{\partial y^2} \right) - \left(M^2 \frac{\rho_f}{\rho_{nf}} \sin^2(\zeta) + \frac{\nu_{nf}}{\nu_f} \Omega \right) u \quad (9)$$

$$u \frac{\partial v}{\partial x} + v \frac{\partial v}{\partial y} = -\frac{\rho_f}{\rho_{nf}} \frac{\partial p}{\partial y} + \nu_{nf} \left(\frac{\partial^2 v}{\partial x^2} + \frac{\partial^2 v}{\partial y^2} \right) \quad (10)$$

$$Pr \left[u \frac{\partial T}{\partial x} + v \frac{\partial T}{\partial y} \right] = \frac{\alpha_{nf}}{\alpha_f} \left(\frac{\partial^2 T}{\partial x^2} + \frac{\partial^2 T}{\partial y^2} \right) + \frac{(\rho C_p)_f}{(\rho C_p)_{nf}} \frac{16\sigma^*}{3k^* k_f} \frac{\partial}{\partial y} \left(\frac{\partial T}{\partial y} \right) T^3 \quad (11)$$

Introducing the stream function [35],

$$u = \frac{\partial \psi}{\partial y}; \quad v = -\frac{\partial \psi}{\partial x} \quad (12)$$

Substitution of equation (12) into equations (9), (10) and (11) differentiate partially equations and making $\frac{\partial}{\partial x \partial y} = \frac{\partial}{\partial y \partial x}$ to eliminate the pressure term,

$$\frac{\nu_{nf}}{\nu_f} (\nabla^4 \psi) + \frac{\partial(\psi, \nabla^2 \psi)}{\partial(x, y)} = - \left(M^2 \frac{\rho_f}{\rho_{nf}} \frac{\sigma_{nf}}{\sigma_f} \sin^2(\zeta) + \frac{\nu_{nf}}{\nu_f} \Omega \right) \nabla^2 \psi \quad (13)$$

$$Pr \left[\frac{\partial \psi}{\partial y} \frac{\partial T}{\partial x} + \frac{\partial \psi}{\partial x} \frac{\partial T}{\partial y} \right] = \frac{\alpha_{nf}}{\alpha_f} \left(\frac{\partial^2 T}{\partial x^2} + \frac{\partial^2 T}{\partial y^2} \right) + \frac{(\rho C_p)_f}{(\rho C_p)_{nf}} \frac{16\sigma^*}{3k^* k_f} \frac{\partial}{\partial y} [T(T_w - T_\infty) + T_\infty^3] \quad (14)$$

The related boundary conditions:

$$\begin{cases} \psi = 0, & \frac{\partial \psi}{\partial y} = x, & T = 1 & \text{at } y = 0 \\ \psi = \frac{a}{e} xy + \frac{1}{2} \gamma y^2, & T = 0 & \text{as } y \rightarrow \infty \end{cases} \quad (15)$$

We quest for solution of equations (13) and (14) as [40]:

$$\psi = xf(y) + g(y), \quad T = \theta(y) \quad (16)$$

where $f(y)$ and $g(y)$ refers to the component normal and tangential of the flow respectively. Using equation (16) in equation (13) and (14), after integration, we find the corresponding differential ordinary equations:

$$\frac{\nu_{nf}}{\nu_f} f'''' + ff'' - f'^2 - \left(M^2 \frac{\rho_f}{\rho_{nf}} \sin^2(\zeta) + \frac{\nu_{nf}}{\nu_f} \Omega \right) f' + C_1 = 0 \quad (17)$$

$$\frac{\nu_{nf}}{\nu_f} g'''' + fg'' - f'g' - \left(M^2 \frac{\rho_f}{\rho_{nf}} \sin^2(\zeta) + \frac{\nu_{nf}}{\nu_f} \Omega \right) g' + C_2 = 0 \quad (18)$$

$$\begin{aligned} Prf\theta' \frac{(\rho C_p)_{nf}}{(\rho C_p)_f} + \frac{k_{nf}}{k_f} \theta'' + \frac{4}{3} Nr\theta''[\theta(\theta_w - 1) + 1]^3 \\ + 4Nr\theta'^2(\theta_w - 1)[\theta(\theta_w - 1) + 1]^2 = 0 \end{aligned} \quad (19)$$

with C_1, C_2 are constant depend on integration. The converted boundary conditions are:

$$\begin{cases} \theta(0) = 1, & g(0) = 0, & g'(0) = 0, & f(0) = 0, & f'(0) = 1 \\ g'(\infty) = \gamma_1 = \frac{b}{e}, & f'(\infty) = \gamma_2 = \frac{a}{e}, & \theta(\infty) = 0. \end{cases} \quad (20)$$

The integration constants C_1 and C_2 obtained using the boundary conditions (20) at infinity, $f'(\infty) = \gamma_2$. An examination of the layer boundary equation (17) divulges that $f(y)$ behaves as $f(y) = \gamma_2 y + A$ as $y \rightarrow \infty$ where A is a constant depending on the displacement of boundary layer. Setting the limit as $y \rightarrow \infty$ and using the condition $g'(\infty) = \gamma_1$ we get,

$$\begin{aligned} C_1 &= \gamma_2^2 + \left(M^2 \frac{\rho_f}{\rho_{nf}} \sin^2(\zeta) + \frac{\nu_{nf}}{\nu_f} \Omega \right) \gamma_2 \\ C_2 &= -\gamma_1 A + \left(M^2 \frac{\rho_f}{\rho_{nf}} \sin^2(\zeta) + \frac{\nu_{nf}}{\nu_f} \Omega \right) \gamma_1 y \end{aligned}$$

The systems of equation take the form:

$$\frac{\nu_{nf}}{\nu_f} f'''' + ff'' - f'^2 - \left(M^2 \frac{\rho_f}{\rho_{nf}} \sin^2(\zeta) + \frac{\nu_{nf}}{\nu_f} \Omega \right) (f' - \gamma_2) + \gamma_2^2 = 0 \quad (21)$$

$$\frac{\nu_{nf}}{\nu_f} g'''' + fg'' - f'g' - \left(M^2 \frac{\rho_f}{\rho_{nf}} \sin^2(\zeta) + \frac{\nu_{nf}}{\nu_f} \Omega \right) (g' - \gamma_1) - \gamma_1 A = 0 \quad (22)$$

$$Prf\theta' \frac{(\rho C_p)_{nf}}{(\rho C_p)_f} + \frac{k_{nf}}{k_f} \theta'' + \frac{4}{3} Nr\theta''[\theta(\theta_w - 1) + 1]^3 + 4Nr\theta'^2(\theta_w - 1)[\theta(\theta_w - 1) + 1]^2 = 0 \quad (23)$$

where $M = \frac{\sigma B_0^2}{\rho_f e}$, $\Omega = \frac{\nu_f}{K_e}$, $\gamma_1 = \frac{b}{e}$, $\gamma_2 = \frac{a}{e}$, $Pr = \frac{\mu_f (\rho C_p)_f}{\rho_f k_f}$, $Nr = \frac{4\sigma^* T_\infty^3}{k^* k_f}$, $\theta_w = \frac{T_w}{T_\infty}$ are, the magnetic parameter, permeability parameter, obliqueness of the flow, parameter of stretching ratio, Prandtl number, parameter of thermal radiation and the heating parameter.

Introducing,

$$g'(y) = \gamma_1 h(y) \quad (24)$$

Equation (22) becomes:

$$\frac{v_{nf}}{v_f} h'' + fh' - f'h - \left(M^2 \frac{\rho_f}{\rho_{nf}} \sin^2(\zeta) + \frac{v_{nf}}{v_f} \Omega \right) (h - y) - A = 0 \quad (25)$$

With the corresponding boundary condition:

$$h'(0) = 0; \quad h(\infty) = 1 \quad (26)$$

The thermo-physical properties for nanofluid are given as [44]:

$$\begin{aligned} \mu_{nf} &= \frac{\mu_f}{(1-\phi)^{2.5}}, & (\rho C_p)_{nf} &= (1-\phi)(\rho C_p)_f + \phi(\rho C_p)_s, \\ \rho_{nf} &= (1-\phi)\rho_f + \phi\rho_s, & \frac{k_{nf}}{k_f} &= \frac{1-\phi + 2\phi \frac{k_s - k_f}{k_s + k_f} \ln\left(\frac{k_s + k_f}{2k_f}\right)}{1-\phi + 2\phi \frac{k_f - k_s}{k_s - k_f} \ln\left(\frac{k_s + k_f}{2k_f}\right)} \end{aligned}$$

Physical Quantities

A mathematical expression for the shear stress τ_w , local heat flux q_w , the local Nusselt number Nu_x and the skin friction coefficient C_f can be expressed as [40,42]:

$$\tau_w = \mu_{nf} \left(\frac{\partial u}{\partial y} \right)_{y=0}, \quad q_w = (q_r)_{y=0} - k_{nf} \left(\frac{\partial T}{\partial y} \right)_{y=0} \quad (27)$$

$$C_f = \frac{\tau_w}{\frac{1}{2} \rho_f (ex)^2}, \quad Nu_x = \frac{xq_w}{k_f (T_w - T_\infty)} \quad (28)$$

In non-dimensional form, they are given by,

$$\frac{1}{2} Re C_{fN} = \frac{1}{(1-\phi)^{2.5}} f''(0), \quad \frac{1}{2} Re C_{fT} = \frac{1}{(1-\phi)^{2.5}} h'(0) \quad (29)$$

$$\frac{Nu}{\sqrt{Re}} = -\theta'(0) \left[\frac{k_{nf}}{k_f} + \frac{4}{3} Nr [\theta(0)(\theta_w - 1) + 1]^3 \right] \quad (30)$$

the local Reynolds number is expressed as $Re = \frac{ex^2}{v_f}$.

Numerical Method

The corresponding differential partial equations (PDE's) are changed to system of ordinary equations (ODEs) (21), (23) and (25) along with the relevant boundary conditions (20) using suitable transformation, then solved using the Bvp4c approach, It's a code of finite difference that employ formula of the three-stage Lobatto IIIa, which is a collocation that offers a C^1 -continuous solution fourth-order accurate in the interval of integration uniformly. The residual of the continuous solution is used for mesh selection and error control. However, this approach is an expanded form of the Runge-Kutta method. This solver has been widely used by other researchers to solve the boundary value problem. In this case, the value $y = y_\infty = 4$ and 5 was used. Because no significant difference in the results for $y > 5$. In other words,

we use [0,5] as the range of this work instead of $[0, \infty[$. The procedure is explained as follows. Let:

$$\begin{aligned} f &= y(1), \quad f' = y(2), \quad f'' = y(3), \quad f''' = yy_1, \quad h = y(4) \\ h' &= y(5), \quad h'' = yy_2, \quad \theta = y(6), \quad \theta' = y(7), \quad \theta'' = yy_3 \end{aligned}$$

$$yy_1 = -\frac{\mu_f \rho_{nf}}{\mu_{nf} \rho_f} \left[y(1)y(3) - y(2)^2 - \left(M^2 \frac{\rho_f}{\rho_{nf}} \sin^2(\zeta) + \frac{v_{nf}}{v_f} \Omega \right) (y(2) - y_2) + y_2^2 \right] \quad (31)$$

$$yy_2 = -\frac{\mu_f \rho_{nf}}{\mu_{nf} \rho_f} \left[y(1)y(5) - y(2)y(4) - \left(M^2 \frac{\rho_f}{\rho_{nf}} \sin^2(\zeta) + \frac{v_{nf}}{v_f} \Omega \right) (y(4) - y) - A \right] \quad (32)$$

$$yy_3 = -\frac{\left[Pr\gamma(1)y(7) \frac{(\rho C_p)_{nf}}{(\rho C_p)_f} + 4Nr\gamma(7)^2(\theta_w - 1)[y(6)(\theta_w - 1) + 1]^2 \right]}{\left[\frac{k_{nf}}{k_f} + \frac{4}{3}Nr[y(6)(\theta_w - 1) + 1]^3 \right]} \quad (33)$$

With the corresponding boundary conditions transformed,

$$\begin{cases} y_0(1), & y_0(2) - 1, & y_0(4), & y_0(6) - 1 \\ y_\infty(2) - y_2, & y_\infty(5) - 1, & y_\infty(6) \end{cases}$$

The procedure of the numerical method used is depicted in Figure 2.

Comparisons of Numerical Results

Table 1 shows the comparison of our work with Mandal et al. [40] and Ramzan et al. [42] for $f''(0)$, $h'(0)$ in the absence of M , ϕ and Ω . It is observed that the accuracy of the method used for our model is quite excellent in agreement with the previous data published in the literature. Table 2 present the validation of our work with Labropulu et al. [4] for $\theta'(0)$ in the absence of M , ϕ , Ω and Nr , with $Pr = 1$. A perfect correlation between the values is found.

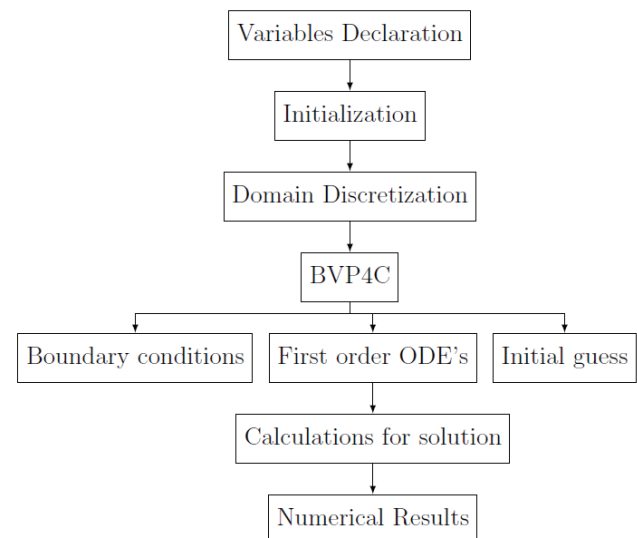


Figure 2. Flow chart of the numerical solution.

Table 1. Comparison of outcome for $f''(0)$ and $h'(0)$ when $M = \Omega = \phi = 0$

γ_2	Present results		Mandal et al. [40]		Ramzan et al. [42]	
	$f''(0)$	$h'(0)$	$f''(0)$	$h'(0)$	$f''(0)$	$h'(0)$
0.1	-0.969387	0.263430	-0.969385	0.263417	-0.96930	0.26339
0.3	-0.849420	0.606337	-0.849419	0.606316	-0.84938	0.60629
0.8	-0.299388	0.934738	-0.299388	0.934728	-0.29935	0.93471
1.0	0.0	1.0	0.0	1.0	0.0	1.0
2.0	2.017502	1.165212	2.017501	1.165218	-	-
3.0	4.729282	1.234655	4.729280	1.234657	-	-

Table 2. Comparison of results for $-\theta'(0)$ when $M = \Omega = \phi = \text{Nr} = 0$ and $\text{Pr} = 1$

γ_2	Present results	Labropulu et al. [4]
	$-\theta'(0)$	$-\theta'(0)$
0.1	0.603491	0.60281
0.3	0.647438	0.64732
0.8	0.757098	0.75709
1.0	0.797884	0.79788
2.0	0.978726	0.97872
3.0	1.132091	1.13209

RESULTS AND DISCUSSION

In order to understand the quantitative effects of the different flow parameters such as magnetic parameter M , angle of inclination ζ , stretching ratio parameter γ_2 , permeability parameter Ω , volume fraction ϕ , on normal velocity, tangential velocity and temperature, we have illustrated Figs. 3-20 for both SWCNTs and MWCNTs. The values of the fixed parameters for the graphical results and the values of Nusselt number and skin friction, are chosen as $M = 0.5$, $\zeta = \pi/2$, $\Omega = 0.5$, $\gamma_1 = 1$, $\gamma_2 = 0.3$, $A = 0.5$, $\phi = 0.03$, $\text{Pr} = 6.7$, $\theta_w = \text{Nr} = 0.5$. Further, the Thermophysical properties consist of density, heat capacitance and thermal conductivity of considered base fluid water, SWCNTs and MWCNTs are mentioned in Tables 3.

Effect of Magnetic Parameter (M)

From Figure 3 we observed a decrease in the normal velocity profiles with increasing the values of magnetic parameter M . This can be explained by the formation of the force of Lorentz which was liable for slowing down the fluid motion and causing the reduction of normal velocity profiles.

The influence of magnetic parameter is discussed through Figure 4. An increase in tangential velocity profiles was observed with increasing values of M near the sheet, while opposite behavior is observed away from the sheet. This can be explained by the formation of the force of Lorentz which was liable for slowing down the fluid motion and causing the reduction of tangential velocity profiles when moving away from the sheet, whereas it increases near the sheet.

Tables 5 and 6 presents the opposite nature of the propagation of the values of skin friction coefficient for normal (C_{f_N}) and tangential (C_{f_T}) components respectively of both SWCNT and MWCNT, it is noticed that the normal component of skin friction is a decreasing functions of magnetic parameter, whereas the contrary is observed for the tangential component of skin friction. One may realize from these tables that MWCNT gives maximum results for tangential skin friction (C_{f_T}) comparing with SWCNT causing a higher drag effect on the surface. In addition, the tangential friction factor increase rate of SWCNT is higher than that MWCNT, which is estimated to be 11.62% and 11.34% for SWCNT and MWCNT, respectively. While an opposite behavior is seen for the normal friction factor decrease rate which evaluated as 35.6% and 36.6% for SWCNT and MWCNT, respectively.

Table 3. Physical properties of base fluid and nanoparticles [40]

Physical properties	Fluid phase (f)	Solid nanoparticle phase (s)	
	Water	SWCNT	MWCNT
$\rho(\text{Kg}/\text{m}^3)$	997.1	2600	1600
$C_p(\text{J}/\text{Kg.K})$	4179	425	796
$k(\text{W}/\text{m.K})$	0.613	6600	3000

Figure 5 reveals the effects of magnetic parameter M on temperature profiles. It is clearly shown that the temperature of the fluid increase with an increase in the magnetic parameter. In addition, the increase of the temperature field is due to the improvement of the Lorentz force, which dissipates more thermal energy in the flowing fluid. That is, thicker thermal boundary layer.

Table 4 shows the effect of magnetic parameter on local Nusselt number. It is evident from Table 4 that the local Nusselt number decreases with an increase in the magnetic field. It can be seen from this Table that SWCNT give the best results compared to MWCNT. This means that the increase in heat transfer is more significant for SWCNT. The Nusselt number reduction rate for SWCNT is 3.98%, while it is 4.01% for MWCNT. The cooling improvement found will be effective for MWCNT.

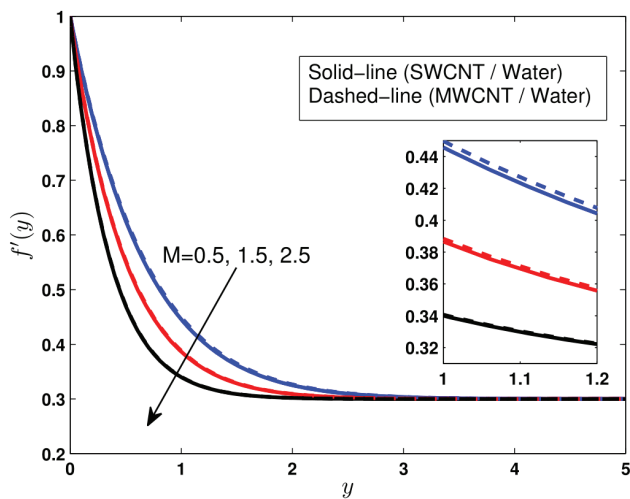


Figure 3. Normal velocity field for variation of M .

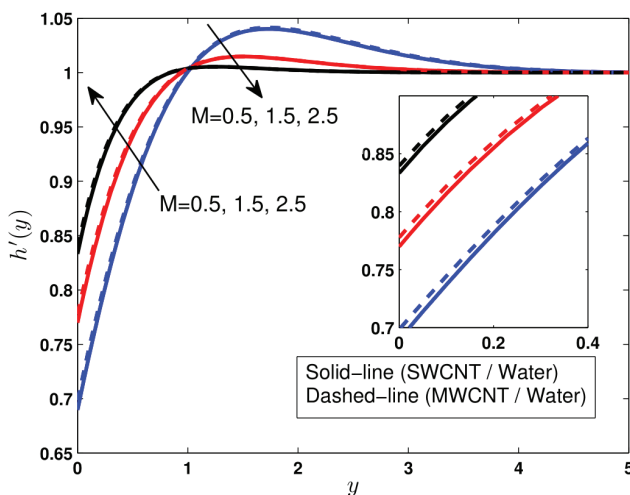


Figure 4. Influence of M on tangential velocity profiles.

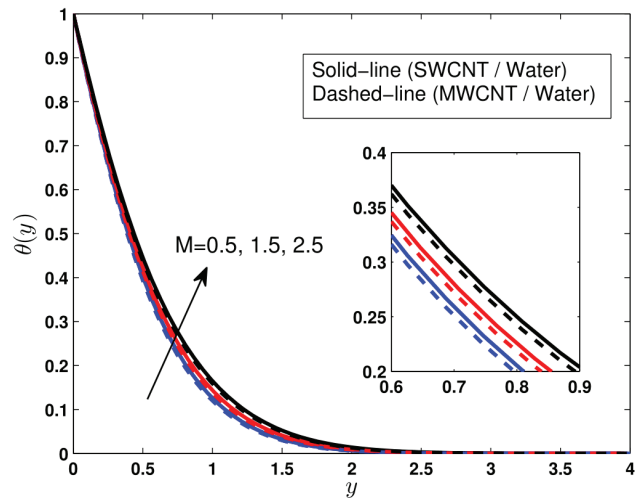


Figure 5. Temperature distribution for variation in M .

Effect of Inclination Angle of Magnetic Field (ζ)

From Figure 6 we observed a decrease in the normal velocity profiles with increasing the values of angle of inclination ζ . This can be explained by the formation of the force of Lorentz which was liable for slowing down the fluid motion and causing the reduction of normal velocity profiles, further, Since $\sin(\zeta)$ is an increasing function when $0 < \zeta < 90$, the strength of magnetic field also increases, and reduces the boundary layer thickness. The same effect is observed by Ref. [41].

Tables 5 and 6 show the contrary nature of the distribution of skin friction coefficient values for the normal (C_{f_N}) and tangential (C_{f_T}) components of both SWCNT and MWCNT. It is noted that the normal component of skin friction is a decreasing function of angle of inclination of magnetic field. These Tables show that MWCNT produces the best results for the tangential skin friction (C_{f_T}) as compared to SWCNT, resulting in a larger drag impact on the surface. Furthermore, the tangential friction factor reduction rate of SWCNT is greater than that of MWCNT, which is predicted to be 0.54% for SWCNT and 0.52% for MWCNT, respectively. The normal friction factor reduction rate, which was 1.35% and 1.40% for SWCNT and MWCNT, respectively, exhibited the opposite tendency.

Figure 7 describes the impact of angle of inclination ζ on tangential velocity profiles. The plots show that an increase of ζ increases the strength of magnetic field, and reduces the boundary layer thickness, which decreases the tangential velocity. One may realize from these Figs. that MWCNTs gives maximum results comparing with SWCNTs this is due to the low density of MWCNT.

The temperature distribution for different values of angle of inclination of external magnetic field ζ is given in Figure 8. It is observed that the temperature distribution increases with an increase in the values of angle of inclination that strengthens the applied magnetic.

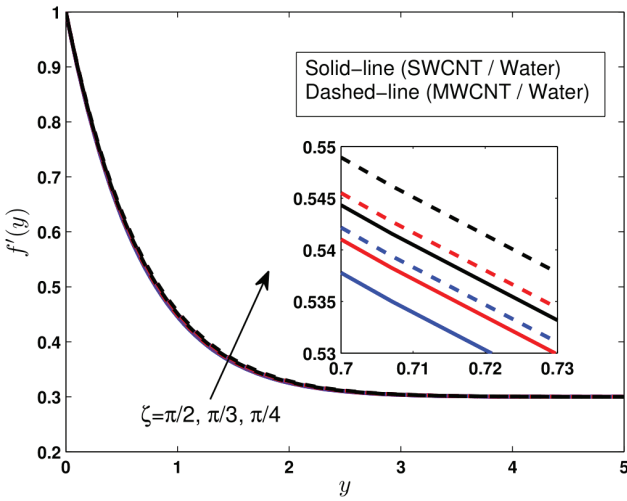


Figure 6. Normal velocity field for variation of ζ .

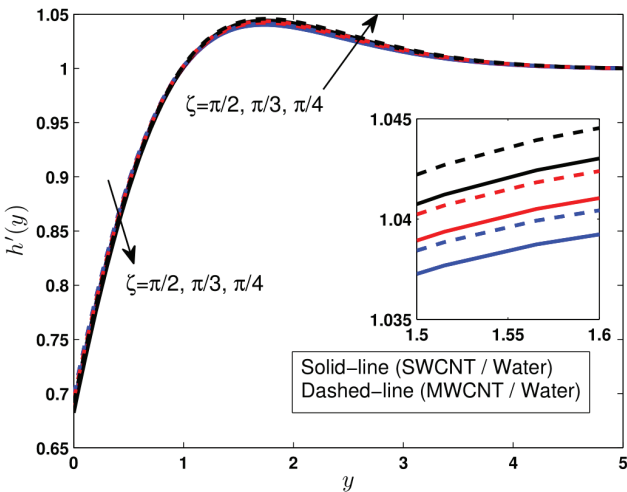


Figure 7. Influence of ζ on tangential velocity profiles.

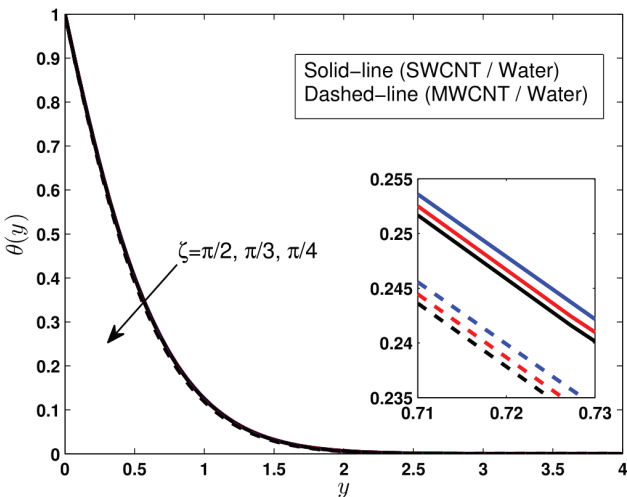


Figure 8. Temperature distribution for variation in ζ .

Effect of Stretching Ratio Parameter (γ_2)

The behavior of the stretching ratio parameter can be described in Figure 9. It is perceived that the normal velocity profiles increases with an increase in the stretching ratio parameter. The stretching rate of the sheet has the potential to increase fluid velocity. As the stretching parameter value increases, the fluid velocity becomes greater than the free stream and the momentum boundary layer becomes thicker.

The tangential velocity for different values of stretching ratio parameter is plotted in Figure 10. We observe that the tangential velocity increase by increasing the value of γ_2 .

Table 5 and 6 reveal the variation of the normal and tangential friction factor (Cf_N), (Cf_T) with the stretching ratio parameter γ_2 . From these tables, we observe the increasing nature of (Cf_N) and (Cf_T) as a function of γ_2 . The same results are verified for both types SWCNT and MWCNT, although the amplification rate value of (Cf_N) found to be larger than (Cf_T), which is 36.53% for SWCNT, 36.51% for MWCNT and 5.18% for SWCNT, 5.14% for MWCNT, respectively.

Figure 11 elaborates the effect of the parameter of stretching ratio γ_2 on temperature. It is seen that temperature distribution decreases with an increase in the stretching ratio parameter. The stretching ratio parameter has the potential to reduce fluid temperature. As the stretching parameter value increases, the thermal boundary layer gets thinner, which reduce the temperature of the fluid. The local Nusselt number for diverse values of stretching ratio parameter for both SWCNT and MWCNT is computed on Table 4. It is perceived that an upsurge in the stretching ratio parameter lead to increase Nu. Similarly, it can be noticed that the heat transport is lower for MWCNT nanofluid. Therefore, the cooling procedure obviously remains high for SWCNT. The percentage of reduction of the local Nusselt number for MWCNT is 4.08%, whereas it is 4.19% for SWCNT.

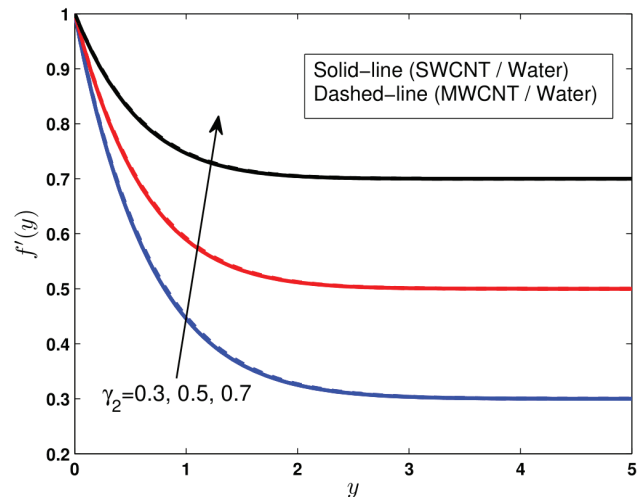


Figure 9. Normal velocity field for variation of γ_2 .

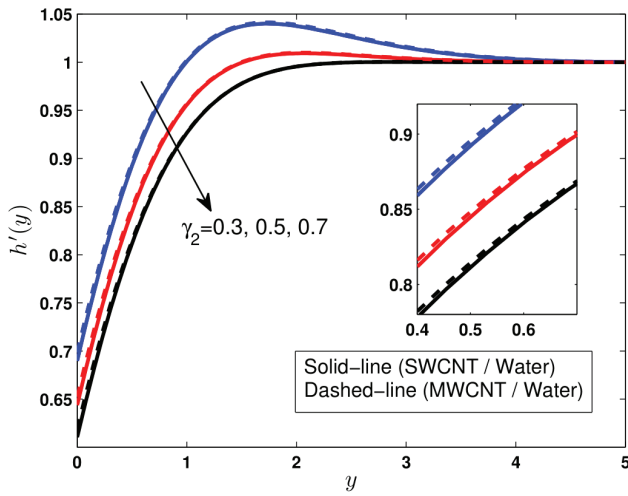


Figure 10. Influence of γ_2 on tangential velocity profiles.

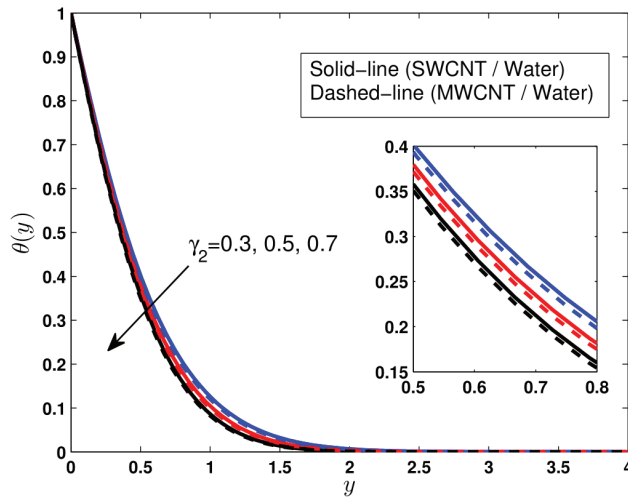


Figure 11. Temperature distribution for variation in γ_2 .

Effect of Permeability Parameter (Ω)

Figure 12 depicts the variation of permeability parameter with the normal velocity. We remark that the increase of Ω follow by the decrease of normal velocity, that's return to the fact that the permeability parameter is inversely proportional to the permeability of the medium, causes a high fluid flow restriction, which results in the retardation of the fluid, and leads to decelerate the fluid in the boundary layer.

Figure 13 gives account of variation of permeability parameter Ω over the tangential velocity. We notice that the tangential velocity decreases with increasing the values of permeability parameter.

In addition, it is also noted that the normal component of skin friction (Cf_N) is a decreasing functions of permeability parameter, while opposite behavior is seen for the tangential component of skin friction (Cf_T). MWCNTs perform the highest tangential skin friction (Cf_T) compared to SWCNTs, resulting in a higher drag effect on the surface.

Thus, in order to achieve optimal velocity of the system, we need to keep Ω within a certain range, otherwise the drag will be too higher for the fluid movement. Moreover, the tangential friction factor increase rate of SWCNT is higher than that MWCNT, which is estimated to be 9.60% and 8.61% for SWCNT and MWCNT, respectively. For the normal friction factor decrease rate was evaluated as 28.75% and 27.91% for SWCNT and MWCNT, respectively.

Figure 14 describes the influence of Ω on temperature distribution. It is readily apparent that temperature increase with an increase in the values of the permeability parameter which make the thermal boundary layer thicker, this is evident from the fact that the porous medium opposes fluid movement and offers resistance to flow.

Table 4 express the changes in local Nusselt number under the positive change in permeability parameter Ω . It depicts a decrease in Nu with the increase in Ω for both SWCNT and MWCNT. The values of Nu for MWCNT

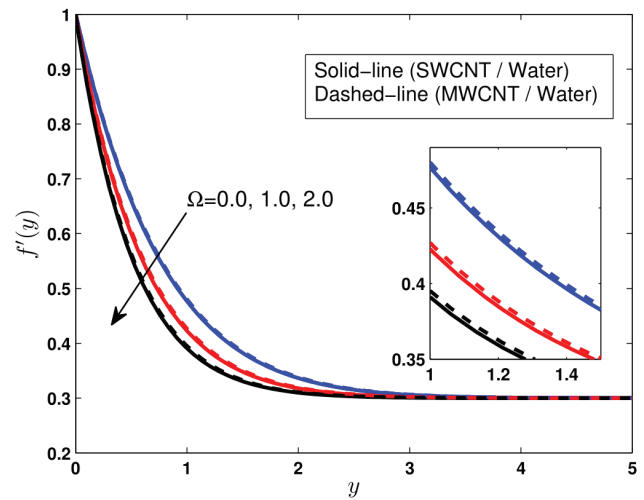


Figure 12. Normal velocity field for variation of Ω .

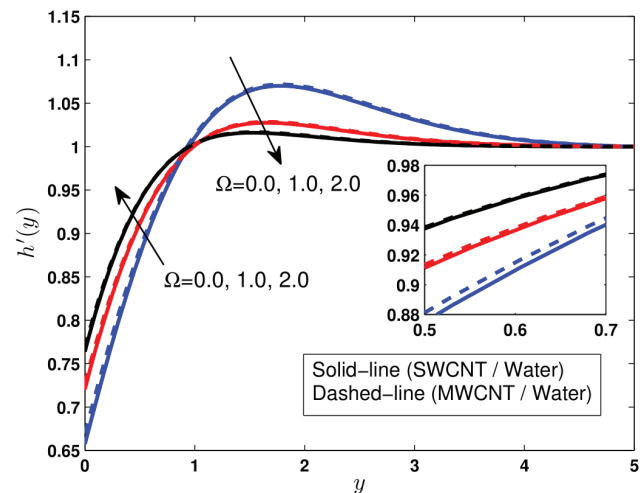


Figure 13. Influence of Ω on tangential velocity profiles.

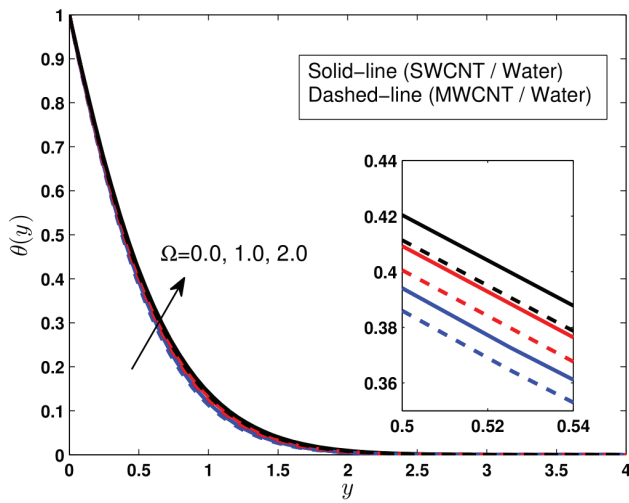


Figure 14. Temperature distribution for variation in Ω .

are slightly lower than that of SWCNT. The reduction rate of Nu in MWCNT is 2.84%, while it is 2.97% in SWCNT composition.

Effect of Volume Fraction of Nanoparticle (ϕ)

The variation of nanoparticle volume fraction is discussed in Figure 15. It is observed that nanoparticles with high concentration possess higher values of normal velocity.

Figure 16 graphically illustrates the influence of volume fraction ϕ on tangential velocity. We analyzed that when increasing the value of volume fraction the tangential velocity increase.

Table 4 shows that with positive inputs of ϕ , the normal component of skin friction (Cf_N) decreases, while the tangential component of skin friction (Cf_T) tend to increase. Although similar results are observed for both SWCNT and MWCNT. The rate of decrease in (Cf_N) evaluated for the SWCNT is 5.24%, while it is 4.11% for the MWCNT.

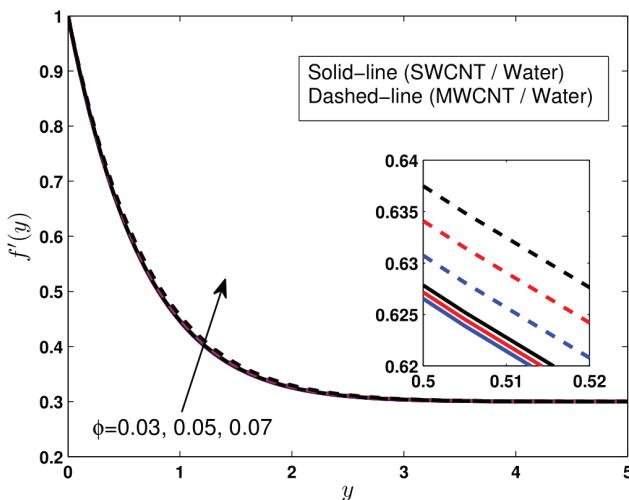


Figure 15. Normal velocity field for variation of ϕ .

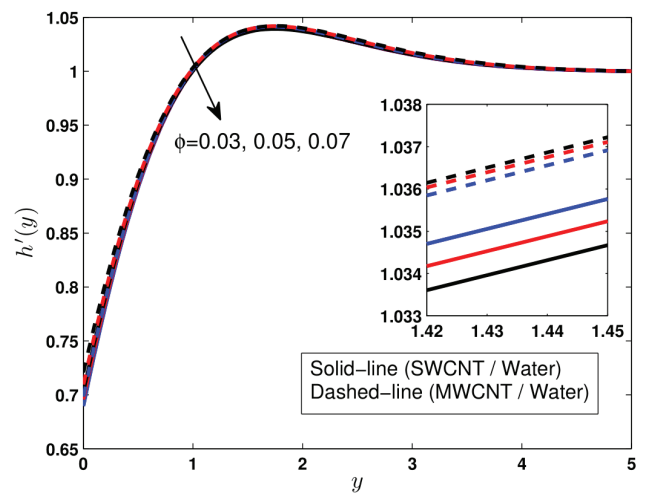


Figure 16. Influence of ϕ on tangential velocity profiles.

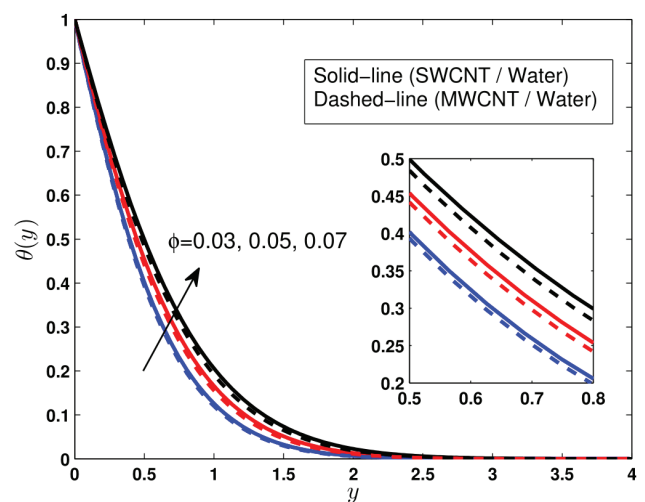


Figure 17. Temperature distribution for variation in ϕ .

The (Cf_T) increase rate estimated for the SWCNT is 6.47%, while it is 7.12% for the MWCNT.

The influence of volume fraction on temperature is explored in Figure 17. We analyzed that the temperature distribution increase with an increase volume fraction of nanoparticle. Physically the thermal conductivity of nanofluids is enhanced due to a rise in the volume fraction of nanoparticles, which make the temperature profile rises.

Table 4 shows that local Nusselt number increases due to the positive changes in ϕ . It is also vital to mention that Nu is better for SWCNT compared to MWCNT. This means that the procedures of cooling our system will happen quickly considering SWCNT. The increase percentage of Nu for SWCNT is 6.59%, while it is 6.45% for MWCNT.

Effect of Radiation Parameter (Nr)

The temperature distribution for diverse values of radiation parameter Nr is given in Figure 18. It is observed that temperature increase with an increase of Nr. In fact, The radiation parameter is the ratio of conductive heat exchange to radiative heat exchange, the increase of the conduction effect inside the thermal limit layer due to the increase of Nr which leads to enhance the temperature. The results qualitatively agree with the report from the literature [45].As a result, utilizing the thermal radiation mechanism, one may simply regulate the rate of heat transfer characteristics.

The local Nusselt number for variation in radiation parameter Nr is presented in table 4. The Nusselt number increase due to Nr improvement for both SWCNT and MWCNT. Here, the maximum values is achieved by the SWCNT compared to MWCNT. The increasing rate of local Nusselt number for SWCNT is about 2.04%, while for the MWCNT is 2.10%.

Effect of Heating Parameter (θ_w)

Figure 19 describes the impact of the heating parameter θ_w on temperature distribution. It is revealed that the temperature increase with an increase of θ_w . This is due to the increase of thermal boundary layer, that is improves the internal heat production which inspires the heat transfer and reinforces the increase of the temperature field. This observation and result are in good agreement with other published article Ref. [46].

Table 4 shows the local Nusselt number for a variety of θ_w inputs. In both SWCNT and MWCNT, Nu is amplified due to the increase in θ_w , although a lower impact is seen for the MWCNT. Therefore, For SWCNT, the increasing rate of Nu is 16.43%, while it is 16.81% for the MWCNT.

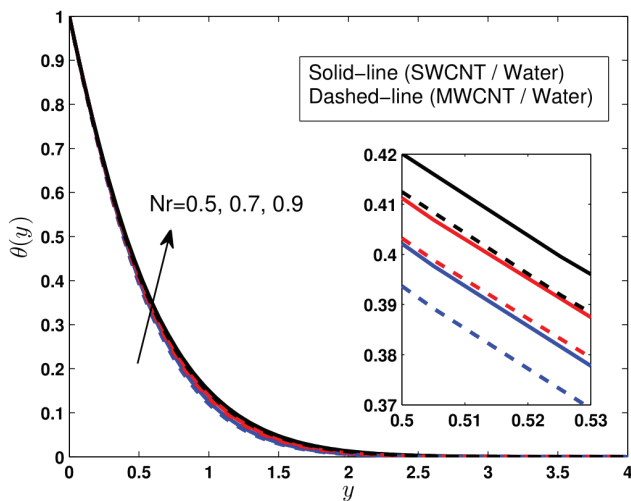


Figure 18. Temperature distribution for variation in Nr.

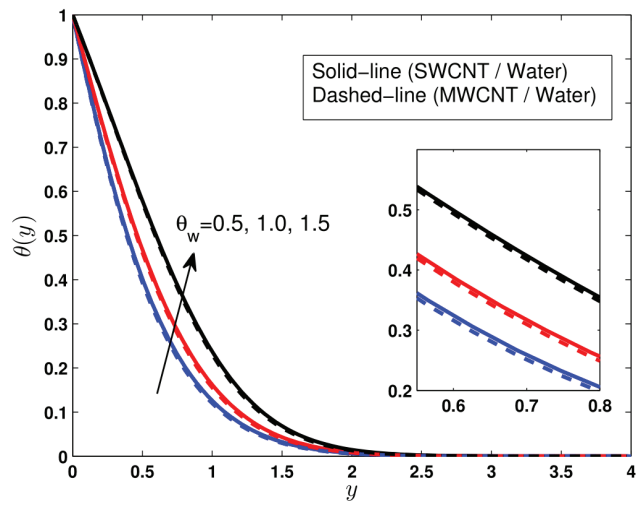


Figure 19. Temperature distribution for variation in θ_w .

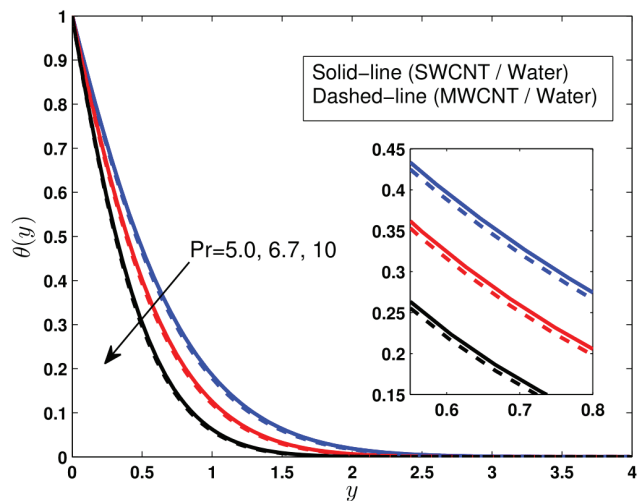


Figure 20. Temperature distribution for variation in Pr.

Effect of Prandtl Parameter (Pr)

The temperature distribution for changing values of Prandtl number is plotted in Figure 20. As noticed. The Prandtl number is, in fact, is the ratio of momentum diffusivity to thermal diffusivity. [47]; for larger Prandtl number, the thermal diffusivity becomes smaller and causing a decrease in the boundary layer thickness, which reduces the temperature. From this results, it can be seen that SWCNTs have a higher temperature than MWCNTs due to their high thermal conductivity.

Table 4 is showing a clear elevation in local Nusselt number with increasing Prandtl number for both SWCNT and MWCNT. It is also evident from the table that Nu is more advanced for the SWCNT compared with MWCNT. The amplification rate of Nu for SWCNT and MWCNT is 47.71% and 47.58%, respectively.

Table 4. Calculation table of local Nusselt number

M	Ω	γ_2	ϕ	Nr	θ_w	Pr	Nu / SWCNT	Nu / MWCNT
0.5	0.5	0.3	0.03	0.5	0.5	6.7	2.354870	2.332430
1.5							2.261203	2.238803
2.5							2.149407	2.127545
0.5	0.0	0.3	0.03	0.5	0.5	6.7	2.393539	2.368890
	1.0						2.322379	2.301585
	2.0						2.269692	2.251234
0.5	0.5	0.5	0.03	0.5	0.5	6.7	2.461129	2.434133
		0.7					2.564429	2.533455
0.5	0.5	0.3	0.05	0.5	0.5	6.7	2.539444	2.508073
			0.07				2.706834	2.669850
0.5	0.5	0.3	0.03	0.7	0.5	6.7	2.405625	2.384289
				0.9			2.454691	2.434386
0.5	0.5	0.3	0.03	0.5	1.0	6.7	2.597675	2.580121
					1.5		3.024404	3.013861
0.5	0.5	0.3	0.03	0.5	0.5	5.0	1.994664	1.976427
						10	2.946430	2.916766

Table 5. Calculation table of normal component of skin friction coefficient.

M	ζ	Ω	γ_2	ϕ	$-1/2R_e C_{fN}$ SWCNT	$-1/2R_e C_{fN}$ MWCNT
0.5	$\pi/2$	0.5	0.3	0.03	1.121224	1.102791
1.5					1.520184	1.506649
2.5					2.103342	2.093596
0.5	$\pi/3$	0.5	0.3	0.03	1.106491	1.087810
	$\pi/4$				1.091565	1.072625
0.5	$\pi/2$	0	0.3	0.03	0.972877	0.960768
		1			1.252587	1.228948
		2			1.481252	1.449148
0.5	$\pi/2$	0.5	0.5	0.03	0.853396	0.839571
			0.7		0.541638	0.532964
0.5	$\pi/2$	0.5	0.3	0.05	1.178873	1.146913
				0.07	1.240665	1.194036

Table 6. Calculation table of tangential component of skin friction coefficient

M	ζ	Ω	γ_2	ϕ	$1/2R_e C_{fT}$ SWCNT	$1/2R_e C_{fT}$ MWCNT
0.5	$\pi/2$	0.5	0.3	0.03	0.744245	0.753748
1.5					0.830751	0.839229
2.5					0.899136	0.905980
0.5	$\pi/3$	0.5	0.3	0.03	0.740278	0.749853
	$\pi/4$				0.736260	0.745925
0.5	$\pi/2$	0	0.3	0.03	0.709603	0.722949
		1			0.777753	0.785244
		2			0.824207	0.829697
0.5	$\pi/2$	0.5	0.5	0.03	0.694663	0.704149
			0.7		0.658674	0.667933
0.5	$\pi/2$	0.5	0.3	0.05	0.790965	0.806775
				0.07	0.842145	0.864240

CONCLUSION

The aim of this paper was to investigate the impact of an inclined magnetic field on oblique stagnation point flow of carbon nanotubes in water as base fluid with nonlinear thermal radiation through a stretching surface in a permeable medium. The objectives were to study the normal velocity, tangential velocity, temperature profiles for both SWCNTs and MWCNTs, for the evaluation of the effect of various physical factors such as the magnetic parameter, angle of inclination of external magnetic field, permeability parameter, volume fraction of nanoparticle and stretching parameter. In this regard, we proposed the governing equations, which are, the momentum equation, and the energy equation. With the help of a suitable transformation the dimensionless differential partial equations (PDE's) have been transformed into differential ordinary equations (ODE's). Then, the equations have been solved numerically using bvp4c approach. The numerical outcomes are provided in graphical and tabular forms and the conclusions are as follows:

- The increasing of permeability parameter, magnetic parameter and angle of inclination reduces the normal and tangential velocity while it enhances the temperature.
- The addition of nanoparticles upsurge the normal velocity and temperature while decreasing the tangential velocity.
- The temperature distribution is enhanced when radiation parameter and heating parameter are increased.
- The normal and tangential velocities are higher for MWCNT compared to SWCNT, the contrary of this trend is found for temperature distribution.
- The normal component of skin friction coefficient values is larger for MWCNT compared to SWCNT as a function of decreasing M , ζ , Ω and ϕ .
- The tangential component of skin friction coefficient values is larger for MWCNT compared to SWCNT as a function of increasing M , ζ , Ω and ϕ .
- Nusselt number rises with rise in radiation parameter, heating parameter and Prandtl number, but decrease with magnetic parameter, permeability parameter, and becomes higher for SWCNT than for MWCNT.

NOMENCLATURE

C_p	Specific heat, J/K
T_∞	Temperature of the ambient, K
k^*	Mean absorption coefficient, m^{-1}
T_w	Temperature of the surface, K
k	Thermal conductivity, W / m.K
K	Permeability of porous medium
Nr	Radiation parameter
M	Magnetic parameter
q_r	Radiative heat flux, W / m^2
Pr	Prandtl number

C_f	Skin friction coefficient
Re	Reynolds number
a, b, e	Constants
A	Displacement coefficient
$f'(y)$	Dimensionless normal velocity
$h'(y)$	Dimensionless tangential velocity

Greek symbols

μ	Dynamic viscosity
α	Thermal diffusivity, m^2 / s
θ	Dimensionless temperature
ρ	Density, kg/m^3
θ_w	Heating parameter
γ_1	Obliqueness of the flow
γ_2	Stretching parameter
Φ	Particle volume fraction
τ_w	Wall shear stress
Ω	Permeability parameter
σ^*	Stefan–Boltzmann constant, W / m^2K^4
ψ	Stream function
ν	Kinematic viscosity, m^2 / s

Subscripts

nf	Indicate nanofluid
f	Indicate fluid
s	Indicate nanoparticle

AUTHORSHIP CONTRIBUTIONS

Authors equally contributed to this work.

DATA AVAILABILITY STATEMENT

The authors confirm that the data that supports the findings of this study are available within the article. Raw data that support the finding of this study are available from the corresponding author, upon reasonable request.

CONFLICT OF INTEREST

The author declared no potential conflicts of interest with respect to the research, authorship, and/or publication of this article.

ETHICS

There are no ethical issues with the publication of this manuscript.

REFERENCES

- [1] Wang CY. The unsteady oblique stagnation point flow. Phys Fluids. 1985;28:2046–2049. [\[CrossRef\]](#)
- [2] Weidman PD, Putkaradze V. Axisymmetric stagnation flow obliquely impinging on a circular cylinder. Eur J Mech B Fluids. 2003;22:123–131. [\[CrossRef\]](#)

- [3] Reza M, Gupta AS. Steady two-dimensional oblique stagnation-point flow towards a stretching surface. *Fluid Dyn Res.* 2005;37:334–340. [\[CrossRef\]](#)
- [4] Labropulu F, Li D, Pop I. Non-orthogonal stagnation-point flow towards a stretching surface in a non-Newtonian fluid with heat transfer. *Int J Therm Sci.* 2010;49:1042–1050. [\[CrossRef\]](#)
- [5] Sarkar S, Sahoo B. Analysis of oblique stagnation point flow over a rough surface. *J Math Anal Appl.* 2020;490:124208. [\[CrossRef\]](#)
- [6] Awan AU, Aziz M, Ullah N. Thermal analysis of oblique stagnation point flow with slippage on second-order fluid. *J Therm Anal Calorim.* 2022;147:3839–3851. [\[CrossRef\]](#)
- [7] Bhuvaneswari M, Eswaramoorthi S, Sivasankaran S, Hussein AK. Cross-diffusion effects on MHD mixed convection over a stretching surface in a porous medium with chemical reaction and convective condition. *Eng Trans.* 2019;67:3–19.
- [8] Maatki C, Ghachem K, Kolsi L, Hussein AK, Mohamed B, Aissia HB. Inclination effects of magnetic field direction in 3D double-diffusive natural convection. *Appl Math Comput.* 2016;273:178–189. [\[CrossRef\]](#)
- [9] Mansour MA, Rashad AM, Mallikarjuna B, Hussein AK, Aichouni M, Kolsi L. MHD mixed bioconvection in a square porous cavity filled by gyrotactic microorganisms. *Int J Heat Technol.* 2019;37:433–445. [\[CrossRef\]](#)
- [10] Ahmed SE, Hussein AK, Mohammed HA, Kayode I, Kolsi L, Zhang X, et al. Viscous dissipation and radiation effects on MHD natural convection in a square enclosure filled with a porous medium. *Nucl Eng Des.* 2014;266:34–42. [\[CrossRef\]](#)
- [11] Hussein AK, Ashorynejad HR, Sivasankaran S, Kolsi L, Kayode I, Sivanandam S, et al. Modeling of MHD natural convection in a square enclosure having an adiabatic square shaped body using Lattice Boltzmann Method. *Alexandria Eng J.* 2016;55:203–214. [\[CrossRef\]](#)
- [12] Pakdee W, Yuvakanit B, Hussein AK. Numerical analysis on the two-dimensional unsteady magnetohydrodynamic compressible flow through a porous medium. *J Appl Fluid Mech.* 2017;10:1153–1159. [\[CrossRef\]](#)
- [13] Singh P, Sinha D. MHD oblique stagnation-point flow towards a stretching Sheet With Heat transfer. *Int J Appl Math Mech.* 2010;6:94–111.
- [14] Borrelli A, Giancesio G, Patria MC. MHD oblique stagnation-point flow of a Newtonian fluid. *Z Angew Math Phys.* 2012;63:271–294. [\[CrossRef\]](#)
- [15] Javed T, Ghaffari A, Ahmad H. Numerical study of unsteady MHD oblique stagnation point flow and heat transfer due to an oscillating stream. *Thermophys Aeromech.* 2016;23:383–391. [\[CrossRef\]](#)
- [16] Awan AU, Abid S, Abbas N. Theoretical study of unsteady oblique stagnation point based Jeffrey nanofluid flow over an oscillatory stretching sheet. *Adv Mech Eng.* 2020;12:1–13. [\[CrossRef\]](#)
- [17] Mohamed MKA, Yasin SHM, Salleh MZ, Alkawasbeh HT. MHD Stagnation Point Flow and Heat Transfer Over a Stretching Sheet in a Blood-Based Casson Ferrofluid With Newtonian Heating. *J Adv Res Fluid Mech Therm Sci.* 2021;82:1–11. [\[CrossRef\]](#)
- [18] Asirvatham LG. Nanofluid heat transfer and applications. *J Therm Eng.* 2015;1:113–115.
- [19] Ravisankar R, Venkatachalapathy VSK, Alagumurthi N. Application of nanotechnology to improve the performance of tractor radiator using Cu-water nanofluid. *J Therm Eng.* 2018;4:2188–2200. [\[CrossRef\]](#)
- [20] Madani K, Maad RB, Abidi-Saad A. Numerical investigation of cooling a ribbed microchannel using nanofluid. *J Therm Eng.* 2018;4:2408–2422. [\[CrossRef\]](#)
- [21] Chand R, Rana GC, Hussein AK. On the onset of thermal instability in a low prandtl number nanofluid layer in a porous medium. *J Appl Fluid Mech.* 2015;8:265–272. [\[CrossRef\]](#)
- [22] Ali B, Hussain S, Nie Y, Habib D, Hussein AK. Finite element investigation of Dufour and Soret impacts on MHD rotating flow of Oldroyd-B nanofluid over a stretching sheet with double diffusion Cattaneo Christov heat flux model. *Powder Technol.* 2021;377:439–452. [\[CrossRef\]](#)
- [23] Ali FH, Hamzah HK, Hussein AK, Jabbar MY, Talebizadehsardari P. MHD mixed convection due to a rotating circular cylinder in a trapezoidal enclosure filled with a nanofluid saturated with a porous media. *Int J Mech Sci.* 2020;181. [\[CrossRef\]](#)
- [24] Ali B, Khan SA, Hussein AK, Thumma T, Hussain S. Hybrid nanofluids: Significance of gravity modulation, heat source/sink, and magnetohydrodynamic on dynamics of micropolar fluid over an inclined surface via finite element simulation. *Appl Math Comput.* 2022;419:126878. [\[CrossRef\]](#)
- [25] Al-Rashed AAAA, Kalidasan K, Kolsi L, Abdelkarim A, Malekshah EH, Kanna PR et al. Three-dimensional investigation of the effects of external magnetic field inclination on laminar natural convection heat transfer in CNT-water nanofluid filled cavity. *J Mol Liq.* 2018;252:454–468. [\[CrossRef\]](#)
- [26] Ashraf MZ, Rehman SU, Farid S, Hussein AK, Ali B, Shah NA, et al. Insight into Significance of Bioconvection on MHD Tangent Hyperbolic Nanofluid Flow of Irregular Thickness across a Slender Elastic Surface. *Mathematics.* 2022;10:1–17. [\[CrossRef\]](#)
- [27] Khan WA, Makinde OD, Khan ZH. Non-aligned MHD stagnation point flow of variable viscosity nanofluids past a stretching sheet with radiative heat. *Int J Heat Mass Transf.* 2016;96:525–534. [\[CrossRef\]](#)

- [28] Mehmood R, Nadeem S, Sher Akbar N. Non-aligned Ethylene-Glycol 30% based stagnation point fluid over a stretching surface with hematite nano particles. *J Appl Fluid Mech.* 2016;9:1359–1366. [\[CrossRef\]](#)
- [29] Khan AU, Nadeem S, Hussain ST. Phase flow study of MHD nanofluid with slip effects on oscillatory oblique stagnation point flow in view of inclined magnetic field. *J Mol Liq.* 2016;224:1210–1219. [\[CrossRef\]](#)
- [30] S Nadeem M, KhanArif R, Khan U. MHD oblique stagnation point flow of nanofluid over an oscillatory stretching/shrinking sheet: existence of dual solutions. *Phys Scr.* 2019;94:075204. [\[CrossRef\]](#)
- [31] Rizwana R, hussain A, Nadeem S. Series solution of unsteady MHD oblique stagnation point flow of copper-water nanofluid flow towards Riga plate. *Heliyon.* 2020;6. [\[CrossRef\]](#)
- [32] Ghasemi SE, Hatami M. Solar radiation effects on MHD stagnation point flow and heat transfer of a nanofluid over a stretching sheet. *Case Stud Therm Eng.* 2021;25:100898. [\[CrossRef\]](#)
- [33] Zainal NA, Nazar R, Naganthran K, Pop I. Unsteady MHD stagnation point flow induced by exponentially permeable stretching/shrinking sheet of hybrid nanofluid. *Eng Sci Technol an Int J.* 2021;24:1201–1210. [\[CrossRef\]](#)
- [34] Nandi S, Kumbhakar B, Sarkar S. MHD stagnation point flow of Fe₃O₄/Cu/Ag-CH₃OH nanofluid along a convectively heated stretching sheet with partial slip and activation energy: Numerical and statistical approach. *Int Commun Heat Mass Transf.* 2022;130:105791. [\[CrossRef\]](#)
- [35] Ghaffari A, Javed T, Majeed A. Influence of Radiation on Non-Newtonian Fluid in the Region of Oblique Stagnation Point Flow in a Porous Medium: A Numerical Study. *Transp Porous Media.* 2016;113:245–266. [\[CrossRef\]](#)
- [36] Khan M, Iqbal Z, Ahmed A. Stagnation point flow of magnetized Burgers' nanofluid subject to thermal radiation. *Appl Nanosci.* 2020;10:5233–5246. [\[CrossRef\]](#)
- [37] Akaje TW, Olajuwon BI. Impacts of Nonlinear Thermal Radiation on a Stagnation Point of an Aligned MHD Casson Nanofluid Flow with Thompson and Troian Slip Boundary Condition. 2021;1:1–15.
- [38] Abbasi A, Gulzar S, Mabood F, Farooq W. Nonlinear thermal radiation and activation energy features in axisymmetric rotational stagnation point flow of hybrid nanofluid. *Int Commun Heat Mass Transf.* 2021;126:105335. [\[CrossRef\]](#)
- [39] Devi R, Poply V, Manimala M. Effect Of Aligned Magnetic Field And Inclined Outer Velocity In Casson Fluid Flow Over A Stretching Sheet With Heat Source. *J Therm Eng.* 2021;7:823–844. [\[CrossRef\]](#)
- [40] Mandal PK, Seth GS, Sarkar S, Chamkha A. A numerical simulation of mixed convective and arbitrarily oblique radiative stagnation point slip flow of a CNT-water MHD nanofluid. *J Therm Anal Calorim.* 2021;143:1901–1916. [\[CrossRef\]](#)
- [41] Sulochana C, Sandeep N, Sugunamma V, Rushi Kumar B. Aligned magnetic field and cross-diffusion effects of a nanofluid over an exponentially stretching surface in porous medium. *Appl Nanosci.* 2016;6:737–746. [\[CrossRef\]](#)
- [42] Ramzan M, Shahmir N, Alotaibi H, Ali H, Ghazwani S, Muhammad T. Thermal performance comparative analysis of nanofluid flows at an oblique stagnation point considering Xue model: a solar application. *J Comput Des Eng.* 2022;9:201–215. [\[CrossRef\]](#)
- [43] Mallikarjuna B, Rashad AM, Hussein AK, Hariprasad Raju S. Transpiration and Thermophoresis Effects on Non-Darcy Convective Flow Past a Rotating Cone with Thermal Radiation. *Arab J Sci Eng.* 2016;41:4691–4700. [\[CrossRef\]](#)
- [44] Nadeem S, Mehmood R, Akbar NS. Oblique stagnation point flow of a casson-nano fluid towards a stretching surface with heat transfer. *J Comput Theor Nanosci.* 2014;11:1422–1432. [\[CrossRef\]](#)
- [45] Agbaje TM, Mondal S, Makukula ZG, Motsa SS, Sibanda P. A new numerical approach to MHD stagnation point flow and heat transfer towards a stretching sheet. *Ain Shams Eng J.* 2016;9:233–243. [\[CrossRef\]](#)
- [46] Kumar A, Sugunamma V, Sandeep N. Impact of Non-linear Radiation on MHD Non-aligned Stagnation Point Flow of Micropolar Fluid over a Convective Surface. *J Non-Equilibrium Thermodyn.* 2018;43:327–345. [\[CrossRef\]](#)
- [47] Hayat T, Shafiq A, Alsaedi A, Asghar S. Effect of inclined magnetic field in flow of third grade fluid with variable thermal conductivity. *AIP Adv.* 2015;5. [\[CrossRef\]](#)